

## Comparison between analog and digital microphone phased arrays for aeroacoustic measurements

Merino-Martínez, Roberto; Sanders, Martinus P.J.; Caldas, Luciano C.; Avallone, Francesco; Ragni, Daniele; de Santana, Leandro D.; Snellen, Mirjam; Simons, Dick G.

**DOI**

[10.2514/6.2018-2809](https://doi.org/10.2514/6.2018-2809)

**Publication date**

2018

**Document Version**

Final published version

**Published in**

2018 AIAA/CEAS Aeroacoustics Conference

**Citation (APA)**

Merino-Martínez, R., Sanders, M. P. J., Caldas, L. C., Avallone, F., Ragni, D., de Santana, L. D., Snellen, M., & Simons, D. G. (2018). Comparison between analog and digital microphone phased arrays for aeroacoustic measurements. In *2018 AIAA/CEAS Aeroacoustics Conference* Article AIAA 2018-2809 American Institute of Aeronautics and Astronautics Inc. (AIAA). <https://doi.org/10.2514/6.2018-2809>

**Important note**

To cite this publication, please use the final published version (if applicable).  
Please check the document version above.

**Copyright**

Other than for strictly personal use, it is not permitted to download, forward or distribute the text or part of it, without the consent of the author(s) and/or copyright holder(s), unless the work is under an open content license such as Creative Commons.

**Takedown policy**

Please contact us and provide details if you believe this document breaches copyrights.  
We will remove access to the work immediately and investigate your claim.

***Green Open Access added to TU Delft Institutional Repository***

***'You share, we take care!' – Taverne project***

**<https://www.openaccess.nl/en/you-share-we-take-care>**

Otherwise as indicated in the copyright section: the publisher is the copyright holder of this work and the author uses the Dutch legislation to make this work public.



# Comparison between analog and digital microphone phased arrays for aeroacoustic measurements

Roberto Merino-Martínez<sup>\*1</sup>, Martinus P. J. Sanders<sup>†2</sup>, Luciano C. Caldas<sup>‡2</sup>, Francesco Avallone<sup>§1</sup>, Daniele Ragni<sup>¶1</sup>, Leandro D. de Santana<sup>||2</sup>, Mirjam Snellen<sup>\*\*1</sup>, and Dick G. Simons<sup>††1</sup>

<sup>1</sup>*Delft University of Technology, 2629 HS Delft, the Netherlands*

<sup>2</sup>*University of Twente, 7522 NB, Enschede, the Netherlands*

Microphone arrays are useful measurement devices for estimating the location and strength of sound sources. Numerous comparative studies have been conducted regarding the performance of acoustic imaging methods in the past, but literature lacks of a systematic investigation on the role of the hardware on the measurements. This research focuses on the performance differences between two 63-microphone arrays: one with digital MEMS (Micro ElectroMechanical Systems) microphones and the other with analog condenser microphones. Both systems are used on an aeroacoustic experiment performed in an anechoic open-jet wind tunnel featuring two airfoils (NACA 0012 and NACA 0018) equipped with trailing-edge serrations. Whereas both arrays provided similar frequency spectra when analyzing trailing-edge noise emissions (which are in agreement with previous research), the analog array seems to offer source maps of higher quality with a higher dynamic range (lower sidelobe level). Moreover, the results of the digital array featuring trailing-edge serrations show a noise increase at the higher frequencies (4 kHz) with respect to the straight-edge case, which is not expected from the findings of previous experimental research. The results of the analog array do not present such behavior. This manuscript is the result of a collaboration project between the University of Twente (UTwente) and Delft University of Technology (TU Delft).

## I. Introduction

Phased microphone arrays are one of the main measurement devices for analyzing aeroacoustic noise sources in applications such as aircraft [1–6], high-speed trains [7, 8], rotating machinery [9, 10], and wind turbines [11, 12]. In combination with acoustic imaging algorithms [13], phased microphone arrays allow for the estimation of the location and strength of sound sources [14, 15].

A microphone array comprises a set of microphones, an electronic amplifier with signal conditioning and an analog to digital converter (ADC) together with frequency filters (typically low-pass). All the channels are connected by cables to the data acquisition system (DAS), which simultaneously samples all the microphone signals, typically using 24-bit resolution for signal recording.

Typical microphone arrays are equipped with high-accuracy analog microphones. For analog systems, the DAS normally contains all the necessary circuitry for the analog-to-digital conversion, see Fig. 1. In

<sup>\*</sup>PhD candidate, Aircraft Noise & Climate Effects section, Faculty of Aerospace Engineering, Kluyverweg 1. AIAA Student Member. E-mail: r.merinomartinez@tudelft.nl

<sup>†</sup>PhD candidate, Faculty of Engineering Technology, Horst building. E-mail: m.p.j.sanders@utwente.nl

<sup>‡</sup>Visiting researcher, Faculty of Engineering Technology, Horst building. E-mail: lucianocaldas@usp.br

<sup>§</sup>Assistant professor, Aeroacoustics section, Faculty of Aerospace Engineering, Kluyverweg 1. E-mail: f.avallone@tudelft.nl

<sup>¶</sup>Assistant professor, Aeroacoustics section, Faculty of Aerospace Engineering, Kluyverweg 1. E-mail: d.ragni@tudelft.nl

<sup>||</sup>Assistant professor, Faculty of Engineering Technology, Horst building. E-mail: leandro.desantana@utwente.nl

<sup>\*\*</sup>Associate professor, Aircraft Noise & Climate Effects section, Faculty of Aerospace Engineering, Kluyverweg 1. E-mail: m.snellen@tudelft.nl

<sup>††</sup>Full professor, Aircraft Noise & Climate Effects section, Faculty of Aerospace Engineering, Kluyverweg 1. E-mail: d.g.simons@tudelft.nl

this configuration, the cables connecting the microphones to the DAS should have good electromagnetic shielding properties, otherwise electromagnetic interference (EMI) will degrade the data, as the signal inside the cable is analog. In general, this results in a rather complicated and expensive system [16].

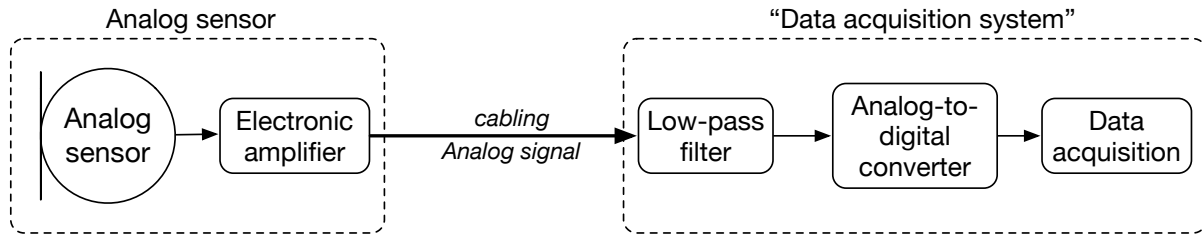


Figure 1: Block diagram illustrating the components of an analog microphone system.

Recent technological advances in digital microphones, such as micro electromechanical systems (MEMS), offer a less expensive and simpler alternative with respect to conventional analog microphones for phased array applications. This type of microphones is normally found in modern cellphones and are, therefore, usually optimized for the human speech frequency range (approximately from 300 Hz to 3 kHz) [16]. Digital sensors are more complex as they have the filtering and ADC embedded, see Fig. 2. A positive feature of this type of systems is that cables transporting digital data are less sensitive to EMI. Another important aspect is the quality of the ADC embedded in each sensor. ADC systems are usually expensive especially if precision (>16-bits) and simultaneous sampling are required. Therefore, having this feature embedded in a cheap sensor can save a reasonable amount of the budget. On the other hand, it is difficult to ensure the precision of this data conversion [16].

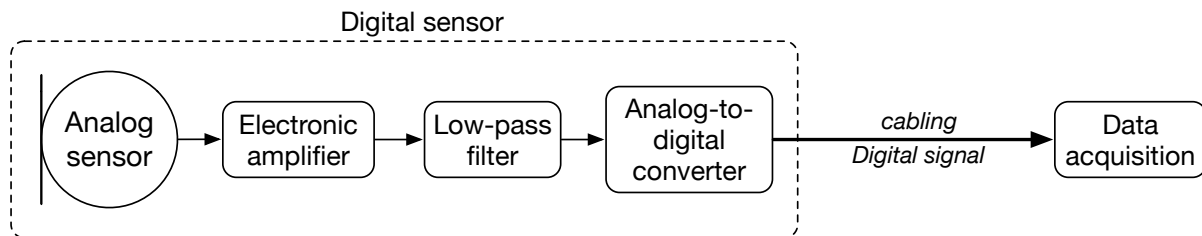


Figure 2: Block diagram illustrating the components of a digital microphone system.

Although many comparative studies have been conducted on the acoustic imaging algorithms themselves [13, 17–20], there is no extended literature evaluating the influence of the hardware used in a phased array. Alexandridis et al. [16] obtained similar results when using an analog and a digital microphone array.

Therefore, the purpose of this paper is to compare the performance of two 63-microphone arrays (one with digital MEMS microphones and the other with analog electret condenser microphones), both with the same microphone distribution, for aeroacoustic measurements. The experiment focuses on the measurement of the turbulent boundary layer trailing-edge (TBL-TE) noise of an airfoil in wind-tunnel tests, which is the dominant noise source for modern wind turbines in normal operational conditions [21, 22]. Trailing-edge serrations [23–31] are one of the most effective passive noise-reduction measures for turbulent-boundary-layer trailing-edge (TBL-TE) noise, currently being applied by wind turbine industry [21, 25–28, 32]. Therefore, the current object of study is the TBL-TE noise of two different airfoil models (NACA 0012 and NACA 0018) equipped with two different serration geometries, as well as of the straight trailing edge case as a baseline. The influence of the airfoil thickness on the performance of the serrations is also investigated. Moreover, the comparison of the experimental results obtained by Arce León et al. [25] with the same airfoil (NACA 0018) and in the same flow conditions, but in another wind-tunnel facility is performed.

The sound spectra measured by both microphone arrays are compared to each other and to the expected results from the literature. The noise reductions due to the addition of the trailing-edge serrations (with respect to the straight-trailing-edge baseline case) obtained by both microphone arrays are also compared. Lastly, the obtained sound source maps by the two arrays are compared while employing identical beamforming algorithm parameters.

This paper is the result of a collaboration project between the University of Twente (UTwente) and Delft University of Technology (TU Delft), both located in the Netherlands.

The paper is structured as follows: section II contains the description of the experimental setup and the phased microphone arrays used. The beamforming method used is briefly explained in section III. The obtained results are gathered in section IV and the conclusions are presented in section V.

## II. Experimental setup

### A. General setup

Aeroacoustic measurements were performed in the Silent Wind-Tunnel facility of the UTwente. The facility is a closed-circuit wind tunnel with an open-jet test section located inside an anechoic chamber of dimensions 6 m (length)  $\times$  6 m (width)  $\times$  4 m (height). In this facility, aeroacoustic measurements can be performed in an anechoic environment (i.e., free-field conditions) for frequencies above 200 Hz. The open-jet test section has rectangular dimensions of 0.9 m (width)  $\times$  0.7 m (height), see Fig. 3. The freestream velocities  $V_\infty$  considered were 20, 30 and 40 m/s with turbulence intensity levels below 0.2%. The maximum velocity corresponds to a chord-based Reynolds number of  $5.26 \times 10^5$  and a Mach number of 0.118, approximately, as in the experiments of Arce León et al. [25].

Two airfoils (NACA 0012 and NACA 0018) with a chord of  $c = 0.2$  m and a span of  $b = 0.7$  m (i.e., equal to the test section height) and manufactured in aluminum were tested in this experiment. The boundary layer was forced to turbulent transition with randomly distributed carborundum roughness elements with a nominal size of 0.6 mm, placed on a tape of 1 cm width, following the recommendations of Braslow et al. [33]. The tape was centered at  $0.2c$  and covered the whole airfoil span on both sides (pressure and suction) of the airfoil, see Fig. 4a. A remote microphone was used to verify that the boundary layer was tripped and that it remains turbulent downstream until the trailing edge.

Two types of solid sawtooth serrations were measured, both manufactured in aluminum and aligned with the flow, retrofitted inside a slot in the trailing edge of each airfoil and with a thickness of 1 mm. The aspect ratio between the serration length  $2h_s$  and the serration width  $\lambda_s$  (see Fig. 4b) was  $2h_s/\lambda_s = 2$  (the same as in [25]), since it has shown to provide the best noise reduction results in a previous research [23]. The two serration geometries considered were:

- **Long solid serrations** with  $\lambda_s = 0.03$  m and  $2h_s = 0.3c = 0.06$  m. These serrations are referred to as *Sr30*.
- **Short solid serrations** with  $\lambda_s = 0.015$  m and  $2h_s = 0.15c = 0.03$  m. These serrations are referred to as *Sr15*.

Hot-wire anemometry (HWA) measurements were performed on both airfoils (for the straight trailing edge configuration) to determine the boundary layer thickness at the trailing edge based on the 95% of the edge velocity ( $\delta_{95}$ ). The average results of these measurements for the three considered flow velocities (20, 30 and 40 m/s) are gathered in Table 1. For a flow velocity of 30 m/s,  $\delta_{95}$  was measured to be 7 mm for the NACA 0012 and 8 mm for the NACA 0018, approximately. The length of the serrations is about 8 and 4 times  $\delta_{95}$  for the *Sr30* and the *Sr15* geometries, respectively. Thus, these serrations are considerably longer than the ones tested by Arce León et al. [25] for the same airfoil and flow conditions, and, hence, are expected to provide higher noise reductions [23].

The coordinate system employed for the experiment is illustrated in Fig. 4a, with the  $x$  axis in the downwind streamwise direction, the  $z$  axis in the spanwise direction pointing upwards, the  $y$  axis perpendicular to the other two axes pointing at the digital microphone array, and the origin placed at the center of the straight trailing edge.

Since both airfoils are symmetric (i.e., they have no camber), the radiated far-field noise is expected to inhibit similar properties on both the pressure and suction sides under no angle of attack. Therefore, only measurements with zero angle of attack ( $\alpha = 0^\circ$ ) are used for comparison in this paper.

Table 1: Boundary layer thickness at the trailing edge ( $\delta_{95}$ ) for both airfoils at different flow velocities.

Flow velocity $V_\infty$ , [m/s]	$\delta_{95}$ for NACA 0012, [mm]	$\delta_{95}$ for NACA 0018, [mm]
20	7.5	8.5
30	7	8
40	6.5	7.5

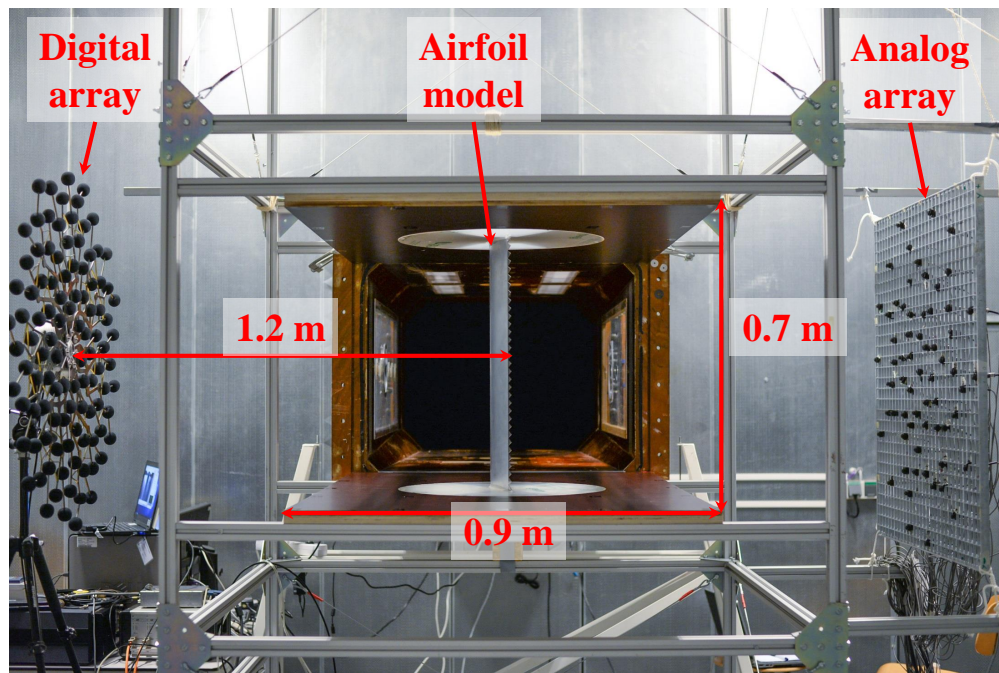


Figure 3: NACA 0012 airfoil installed in the open-jet test section (front view) with both microphone arrays (*Digital* on the left and *Analog* on the right).

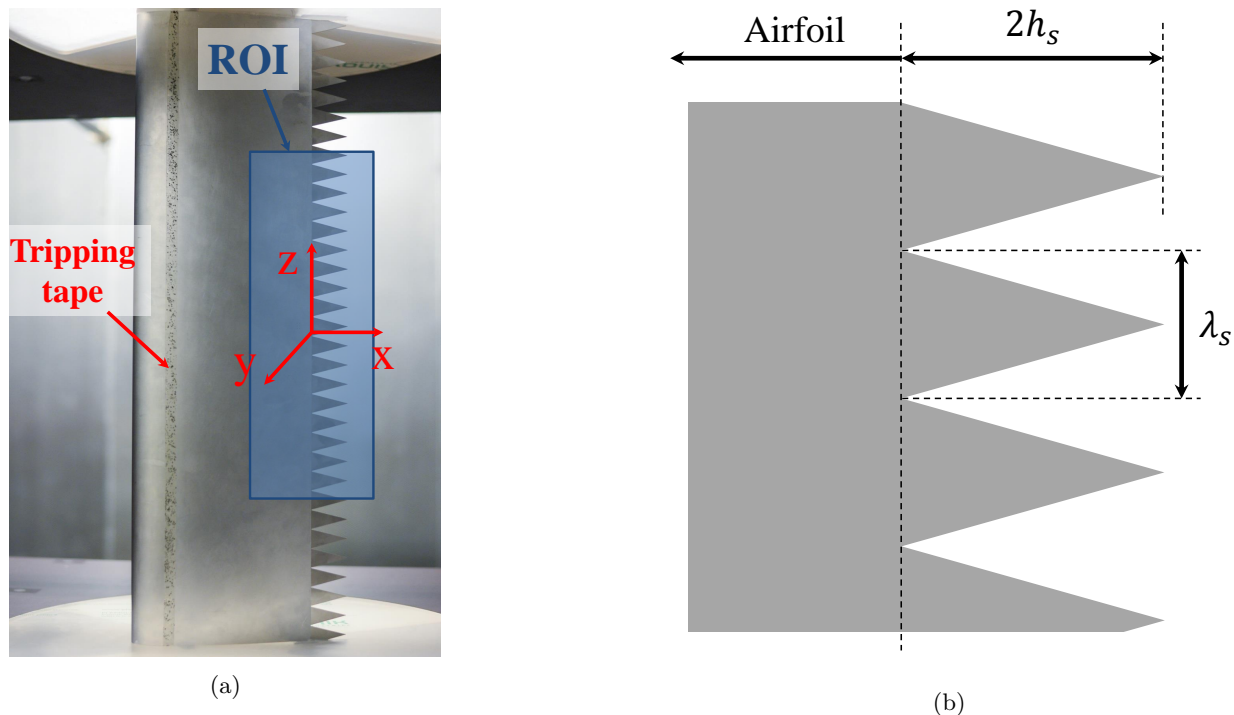


Figure 4: (a) Coordinate system adopted and representation of the region of integration (ROI) size and location (shaded in blue). The location of the tripping tape is also indicated for this example of the NACA 0012 airfoil with  $Sr30$  serrations. (b) Definition of the serration geometry parameters.

## B. Phased microphone arrays

Two phased microphone arrays were employed to analyze the TBL–TE noise emissions placed at opposite side of the airfoil, as shown in Fig. 3, and at a distance of  $h = 1.2$  m from the airfoil trailing edge:

- A CAE Systems M–112 Bionic Array [34] (Fig. 3 left) consisting of 112 Invensense INMP441 digital MEMS microphones with an integrated data acquisition system inside the hub of the array. The frequency range of the microphones spans from 10 Hz to 24 kHz. Digital time data is directly saved to a laptop computer at a sampling frequency of 48 kHz using the array’s integrated FPGA (Field–Programmable Gate Array) system. The microphones are recessed inside small cavities, flush–mounted with the array mounting structure. Thus, sound reflections from the array structure can be expected at the microphones. From the total of 112 microphones, 63 were selected to compare the results with the other array, see Fig. 5a. Henceforth, this array is referred to as *Digital* array.
- A reconfigurable microphone array (Fig. 3 right) consisting of 63 PUI Audio POM–2735P–R analog condenser microphones [35] (with a data acquisition developed at TU Delft). These microphones have a sensitivity of  $-35 \pm 2$  dB (ref. 1 V/Pa) and a frequency range of 20 Hz to 25 kHz. The microphone distribution approximated the selected undersampled geometry of the *Digital* array, see Fig. 5b. The sampling frequency employed was 50 kHz. Each microphone was previously calibrated using a calibrated pistonphone emitting at 250 Hz. The performance of this array has already been compared with computational aeroacoustic methods, with successful results [29, 36]. Henceforth, this array is referred to as *Analog* array.

Both arrays have an approximate diameter of  $D = 1$  m, see Fig. 5. The approximate costs of both microphone types are similar and in the order of 1 euro per piece. Therefore, the comparison between both systems is considered as representative.

The centers of both arrays were aligned with the center of the trailing edge of the airfoil ( $x = z = 0$  m). Both microphone distributions were almost identical, but the *Analog* array presented a small rotation with

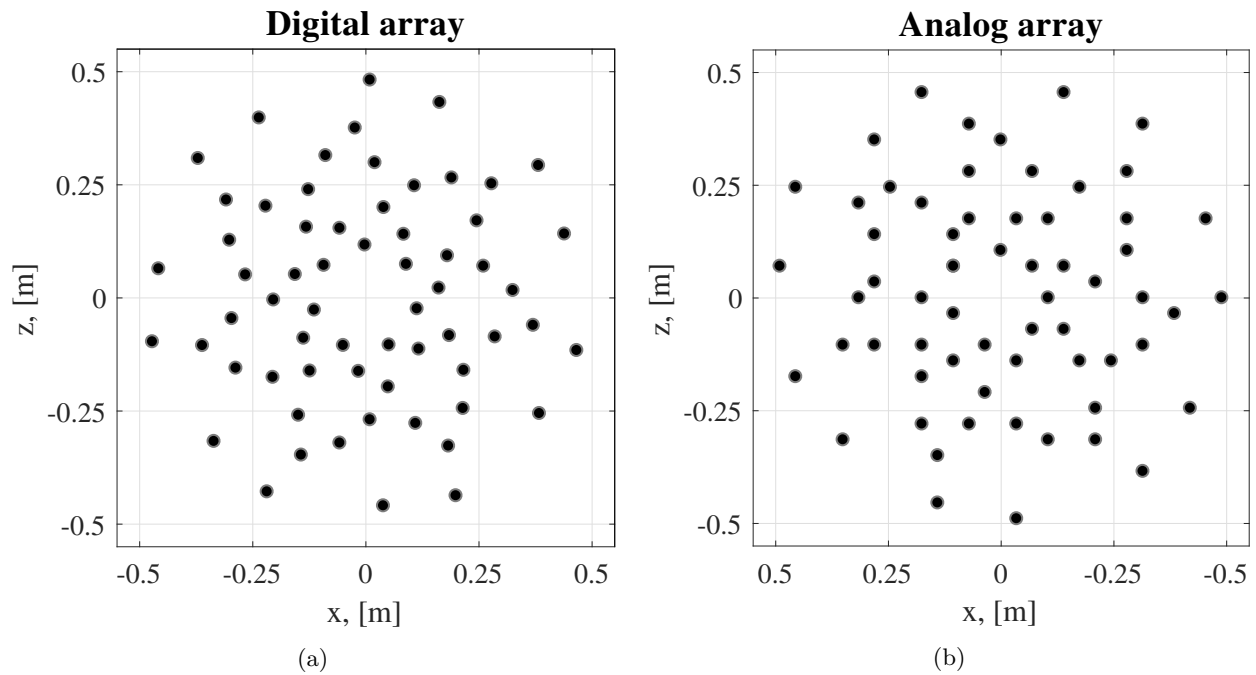


Figure 5: Microphone distribution for (a) The *Digital* phased microphone array. (b) The *Analog* phased microphone array. Note that the  $x$  axis is reversed for better comparison.

respect to the *Digital* array. The effect of this small difference, however, is expected to be negligible.

Raw time signals were simultaneously acquired by both arrays. For each measurement, 60 s of data were recorded. The acoustic data was averaged using time blocks of 4096 samples (corresponding to a time interval of  $T_h = 85.33$  ms for the *Digital* array and  $T_h = 81.92$  ms for the *Analog* array) and windowed using a Hanning weighting function with 50 % data overlap following Welch's method [37]. With these values, the frequency resolution for both arrays is approximately  $\Delta f \approx 12$  Hz. The frequency range of interest was selected to be between 1 kHz and 5 kHz as in previous experiments [25–28].

### III. Methodology

#### A. Source Power Integration extended to line sources (SPIL)

Conventional frequency domain beamforming (CFDBF) [14, 15] is a widely-used, robust and fast algorithm. This method assumes the presence of point sound sources and, for well-separated sources, CFDBF provides the correct source sound pressure level  $L_p$  [12]. However, in practice, sound sources are typically distributed over extended regions, such as a trailing edge, and conventional beamforming methods do not yield the correct emitted noise levels.

To mitigate this issue, different integration methods have been proposed [38]. The Source Power Integration (SPI) technique [15, 39] extended to line sources (SPIL) [38] was introduced in order to reduce the influence of the array point spread function (PSF). This technique is specifically tailored for line sources, such as trailing-edge noise. The SPIL method sums the source autopowers  $A_j$  in a selected region of integration (ROI) of the source map obtained by CFDBF, containing  $J$  grid points. It then corrects the result with a scaling factor obtained by performing a simulation for a line source located within the ROI at the expected location of the line source [38]. In practice, a large number  $K$  of simulated incoherent point sources of equal power level are placed along the expected location of the experimental line source with steering vectors  $\mathbf{g}_k$ ,  $k \in [1 \cdots K]$  [15]. The integrated source power  $P_{\text{exp}}$  (per frequency  $f$ ) on the ROI is calculated as:

$$P_{\text{exp}} = \sum_{j=1}^J A_{j,\text{exp}} \frac{P_{\text{sim}}}{\sum_{j=1}^J A_{j,\text{sim}}} = \sum_{j=1}^J (\mathbf{g}_j^* \mathbf{C} \mathbf{g}_j) \frac{P_{\text{sim}}}{\sum_{j=1}^J \left( \mathbf{g}_j^* \left( \sum_{k=1}^K \mathbf{g}_k \mathbf{g}_k^* \right) \mathbf{g}_j \right)}, \quad (1)$$

where  $P_{\text{sim}}$  is the sound power due to all the  $K$  simulated sources,  $J$  is the number of grid points in the ROI,  $\mathbf{C}$  is the cross-spectral matrix (CSM), and  $A_{j,\text{exp}}$  and  $A_{j,\text{sim}}$  are the experimental and simulated CFDBF results, respectively.

Mean flow convection of the sound was taken into account in the steering vector formulation using an average Mach number of the flow following the approach proposed by Amiet [40]. Moreover, the main diagonal of the CSM was removed in order to mitigate the effect of the incoherent background noise from the wind tunnel [15].

## B. Beamforming parameters

A scan grid covering a range from  $x = -0.3$  m to  $x = 0.3$  m and from  $z = -0.45$  m to  $z = 0.45$  m, i.e., covering the whole airfoil, was defined for both arrays. A constant spacing between grid points  $\Delta x$  of 0.01 m was selected. Both datasets were processed with the same software developed in-house.

Following the guidelines specified in [38], a ROI was defined in order to apply the SPIL method ranging from  $x = -0.07$  m to  $x = 0.07$  m and from  $z = -0.2$  m to  $z = 0.2$  m, see Fig. 4a. A simulated line source was considered at the trailing edge position ( $x = 0$  m and from  $z = -0.2$  m to  $z = 0.2$  m). The corners of the airfoil's trailing edge were excluded from the ROI in order to mitigate the influence of any potential "corner" sources due to interaction of the airfoil with the boundary layers of the wind-tunnel walls [41, 42].

# IV. Results

## A. Comparison of beamforming source plots

As an illustrative example, the CFDBF source plots obtained by both arrays for the NACA 0012 airfoil with straight trailing edge at  $\alpha = 0^\circ$  and  $V_\infty = 30$  m/s and a one-third-octave frequency band centered at 2 kHz are presented in Fig. 6. Whereas, both beamforming plots present a similar source distribution (a vertical line source located at the trailing edge of the airfoil,  $x = 0$  m) and comparable peak values, the beamform map provided by the *Digital* array (Fig. 6a) has higher sidelobes (i.e., spurious sources) than the one by the *Analog* array (Fig 6b). Results for the same configuration but at a one-third-octave frequency band centered at 4 kHz are presented in Fig. 7. Once again the results from the *Analog* array present less sidelobes than those from the *Digital* array. Slightly lower peak levels (about 1.5 dB lower) are observed in the source plot by the *Analog* array compared to the *Digital* one. Similar behaviors were found for other frequency ranges and airfoil configurations.

The spatial resolution of a given array improves with increasing frequency following the Rayleigh resolution limit [43]:

$$\theta_{\text{scan},0} \approx 1.22 \frac{c_0}{Df}, \quad (2)$$

where  $\theta_{\text{scan},0}$  represents the minimum angular distance at which two sound sources can be separated,  $D$  is the array diameter,  $c_0$  is the sound speed and  $f$  is the sound frequency.

For practical applications, it is common to consider the spatial resolution  $R(f)$  in meters rather than the angular resolution  $\theta_{\text{scan},0}$  in radians [44]. For a scan plane situated at a distance  $h$  from the array plane, the minimum distance between two sources for which they can be solved is approximately

$$R(f) \approx h \tan(\theta_{\text{scan},0}) \approx 2h \tan\left(\frac{\theta_{\text{scan},0}}{2}\right) \approx 2h \tan\left(0.61 \frac{c}{Df}\right). \quad (3)$$

Both arrays show similar spatial resolutions, since this parameter mostly depends on the array aperture and the microphone distribution [45], and these features are almost identical for both arrays, see Fig. 5.

To further investigate the dynamic range of both arrays, this parameter was calculated for both arrays when analyzing the NACA 0012 airfoil with straight trailing edge at  $\alpha = 0^\circ$  and  $V_\infty = 30$  m/s. Since the spatial resolution of an array improves with increasing frequency, see Eq. (2), only the results further away than a distance  $R(f)$  from the trailing edge of the airfoil ( $x = 0$  m) and within a scan grid going from

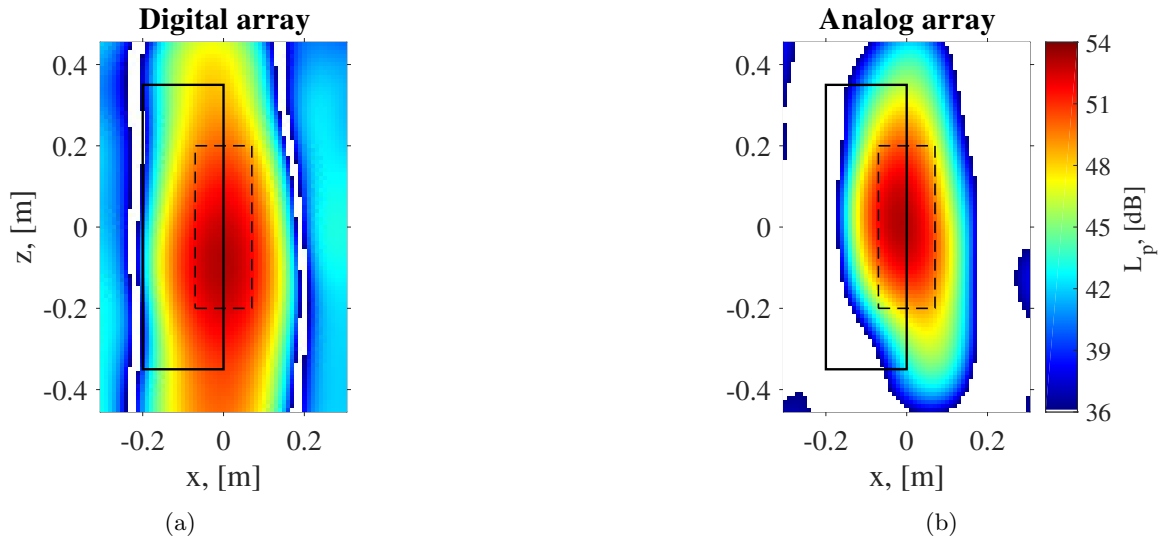


Figure 6: CFDBF source plots obtained for the NACA 0012 airfoil with straight trailing edge at  $\alpha = 0^\circ$  and  $V_\infty = 30$  m/s for: (a) the *Digital* array and (b) the *Analog* array. The results correspond to a one-third-octave frequency band centered at 2 kHz. The airfoil location is denoted by a solid rectangle and the ROI by a dashed rectangle using same orientation as depicted in Fig. 4a. The results for the *Analog* array have been mirrored with respect to the  $z$  axis for an easier comparison.

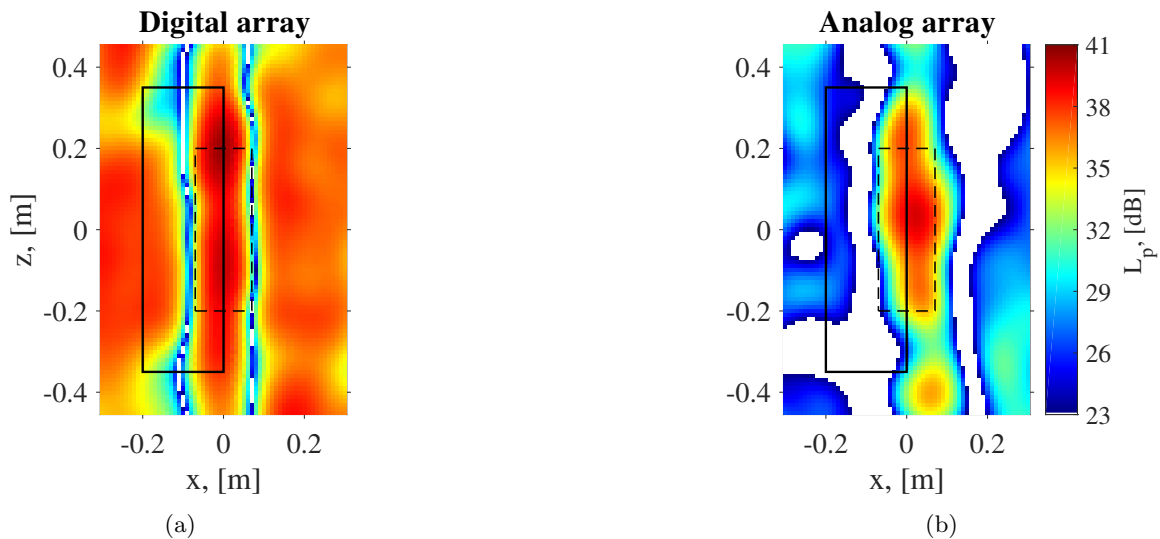


Figure 7: CFDBF source plots obtained for the NACA 0012 airfoil with straight trailing edge at  $\alpha = 0^\circ$  and  $V_\infty = 30$  m/s for: (a) the *Digital* array and (b) the *Analog* array. The results correspond to a one-third-octave frequency band centered at 4 kHz. The airfoil location is denoted by a solid rectangle and the ROI by a dashed rectangle using same orientation as depicted in Fig. 4a. The results for the *Analog* array have been mirrored with respect to the  $z$  axis for an easier comparison.

$x = -0.6$  m to  $x = 0.6$  m are considered, i.e., for  $x \in -0.6 \text{ m} \leq x \leq -R(f) \cup R(f) \leq x \leq 0.6 \text{ m}$  (see Fig. 8a) and for  $z \in -0.35 \text{ m} \leq z \leq 0.35 \text{ m}$ . The dynamic range is defined as the difference between the peak level found in the trailing-edge region ( $x \in -R(f) \leq x \leq R(f)$ ) and the peak sidelobe level in the sidelobe search area defined in Fig. 8a (colored in orange). Thus, different search areas are considered for each frequency. These boundaries were selected in order to include potential sidelobes, but to exclude extraneous noise sources from the wind-tunnel facility located further away as much as possible.

The dynamic ranges obtained for both arrays for these conditions are presented in Fig. 8b. Both microphone arrays show similar behaviors between 1 kHz and 1.6 kHz and for frequencies higher than 8 kHz. Between 2 kHz and 6 kHz, however, the dynamic range of the *Analog* array is considerably higher (approximately 4.8 dB in that range) than the one of the *Digital* array. The exact reason for this difference is unknown, but could be caused by the different microphone electronics as well as different DAS used.

The relatively low dynamic range for frequencies below 1.6 kHz can be explained because of the limited sidelobe search area for low frequencies since  $R \approx 0.53$  m for 1 kHz. In general, higher frequencies present higher sidelobes [14], and hence lower dynamic ranges. The fact that both arrays present very similar values for the 8 kHz and 10 kHz one-third-octave bands may be due to the lower SNR at those frequencies for trailing-edge noise [25]. Therefore, those two frequencies probably correspond to background noise.

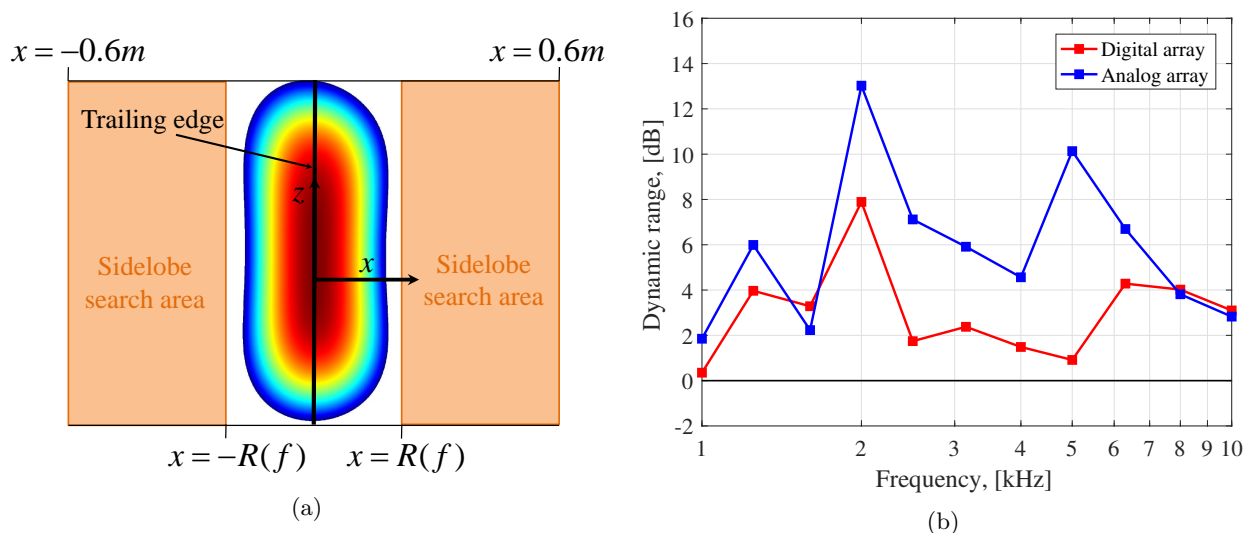


Figure 8: (a) Diagram explaining the search areas for sidelobes (colored in orange). (b) Dynamic range of both microphone arrays for the NACA 0012 airfoil with straight trailing edge at  $\alpha = 0^\circ$  and  $V_\infty = 30$  m/s.

## B. Comparison of integrated sound spectra

A comparison of the integrated sound spectra in the ROI defined in Fig. 6 is presented in Fig. 9 for the *Digital* array (left) and for the *Analog* array (right). Both plots correspond to the NACA 0018 airfoil at  $\alpha = 0^\circ$  and  $V_\infty = 40$  m/s and the three trailing-edge geometries (straight, *Sr15* and *Sr30*). The absolute values of the three spectra for both arrays are comparable. This confirms that, despite the higher presence of sidelobes for the *Digital* array results (see Figs. 6 and 7), the SPIL method reduces their influence by integrating the results in a ROI. The main difference observed in Fig. 9 is that the *Digital* array shows a crossover frequency around 3.5 kHz after which the spectra from both serrated cases show higher noise emissions than the straight trailing-edge baseline case. A noise increase of about 5 dB is measured for the 4 kHz one-third-octave band and about 2 dB for the 5 kHz band. This phenomenon does not occur for the *Analog* array, where only a noise increase of about 2 dB is observed for the band centered at 5 kHz. Such noise increase after a crossover frequency was not observed by an analogous experiment by Arce León et al. [25, 27] with the same airfoil and flow conditions. A noise increase was only observed when a serration-flow misalignment angle was present [26]. This phenomenon might be related to the fact that digital microphones are normally optimized for the human speech frequency range (300 Hz to 3 kHz), as aforementioned.

In order to investigate this phenomenon in more detail, the relative differences with respect to the straight

trailing edge for both serration geometries and both microphone arrays are presented in section IV.C.

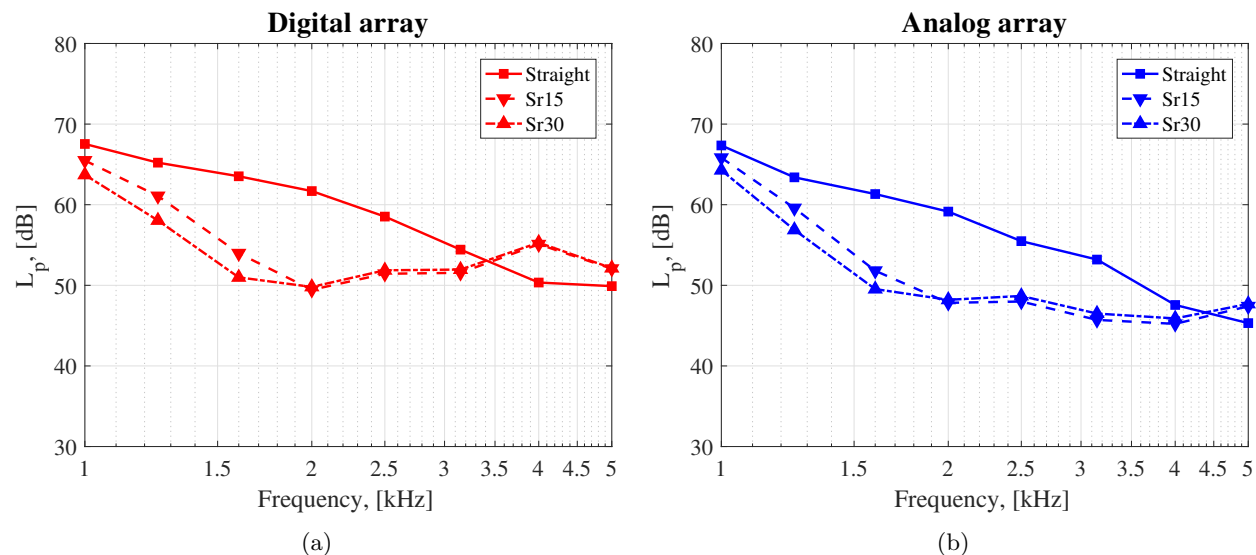


Figure 9: Integrated sound spectra for the three trailing-edge geometries for the NACA 0018 airfoil at  $\alpha = 0^\circ$  and  $V_\infty = 40$  m/s for: (a) the *Digital* array and (b) the *Analog* array.

### C. Comparison of noise reductions

This section presents the calculated noise reduction levels  $\Delta L_p = L_{p,STE} - L_{p,s}$ , where  $L_{p,STE}$  and  $L_{p,s}$  refer to the straight and serrated trailing edge cases, respectively. With this criterion,  $\Delta L_p > 0$  corresponds to a noise reduction and vice versa.

Figure 10 depicts the  $\Delta L_p$  values for the NACA 0012 airfoil at  $\alpha = 0^\circ$  and freestream velocities  $V_\infty$  of 20, 30 and 40 m/s (from left to right). It can be observed that when the freestream velocity increases, the frequency at which the maximum noise reduction is obtained increases. This behavior agrees with the theory [23]. The maximum  $\Delta L_p$  also increases with  $V_\infty$ , up to a maximum of about 16 dB at 40 m/s. Both microphone arrays show similar results for the whole frequency range of interest, except at 2 kHz, where the *Digital* array presents a lower noise reduction. Another interesting difference is that for  $V_\infty = 20$  m/s and  $V_\infty = 30$  m/s, the results from the *Digital* array show negative values of  $\Delta L_p$  for 4 kHz and 5 kHz, i.e., a noise increase. The *Analog* array only presents minor noise increases at 5 kHz which can be due to accuracy reasons and the poorer SNR at that frequency. Both serration geometries seem to provide similar noise-reduction performances, with the *Sr30* configuration performing slightly better than the *Sr15* in most cases up to 3 kHz.

Figure 11 illustrates the  $\Delta L_p$  values for the NACA 0018 airfoil at  $\alpha = 0^\circ$  and freestream velocities of 20, 30 and 40 m/s (from left to right). Once again, when the freestream velocity increases, the frequency at which the maximum noise reduction is obtained increases. This time, a maximum  $\Delta L_p$  value of about 12 dB is obtained. For this configuration larger differences are present between the results of both arrays, especially at 1.6 kHz and  $V_\infty = 20$  m/s and for frequencies higher than 2.5 kHz in the case with  $V_\infty = 40$  m/s. In general, the *Digital* array shows higher noise reductions for frequencies between 1.2 kHz and 2 kHz but lower (and even negative)  $\Delta L_p$  values for frequencies higher than 3 kHz. In this case, the *Sr30* geometry also shows slightly better performance than the *Sr15*, especially at low frequencies.

The higher noise reduction levels obtained by the NACA 0012 airfoil compared with the NACA 0018 airfoil are probably because of the different pressure gradient (due to the lower thickness of the first) and, therefore, a closer resemblance to a flat plate [23, 46] for the NACA 0012 airfoil.

Figures 12 and 13 present the noise reductions  $\Delta L_p$  obtained by the *Sr30* serrations measured by both microphone arrays for the NACA 0012 and NACA 0018 airfoils, respectively. In this case, the frequency axes are expressed in terms of the Strouhal number based on the boundary layer thickness (see Table 1)  $St = f\delta_{95}/V_\infty$ . Only the *Sr30* geometry was considered for simplicity reasons and because similar results were obtained for the *Sr15* case, see Figs. 10 and 11.

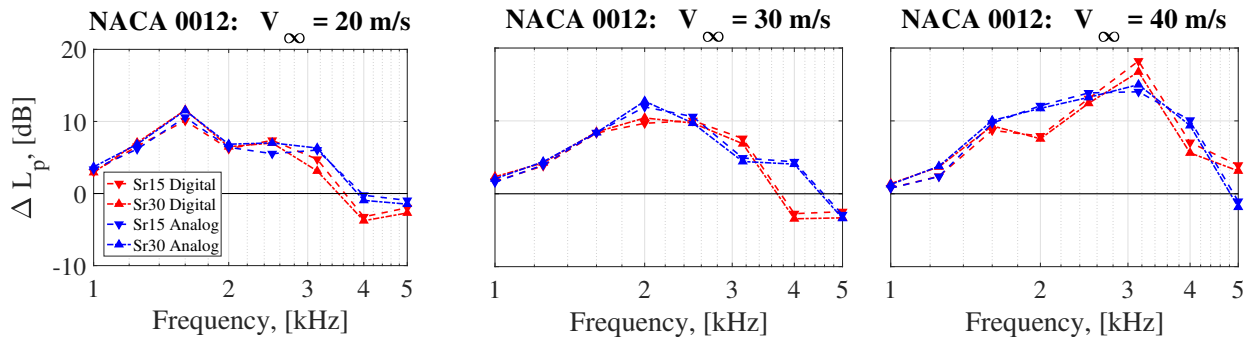


Figure 10: Relative integrated sound spectra with respect to the straight trailing edge for both serration geometries and both microphone arrays for the NACA 0012 airfoil at  $\alpha = 0^\circ$  and freestream velocities of 20, 30 and 40 m/s (from left to right).

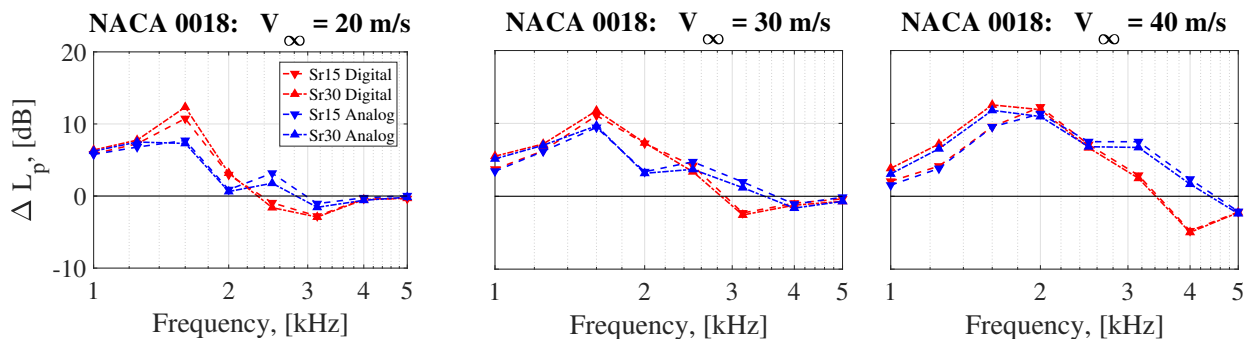


Figure 11: Relative integrated sound spectra with respect to the straight trailing edge for both serration geometries and both microphone arrays for the NACA 0018 airfoil at  $\alpha = 0^\circ$  and freestream velocities of 20, 30 and 40 m/s (from left to right).

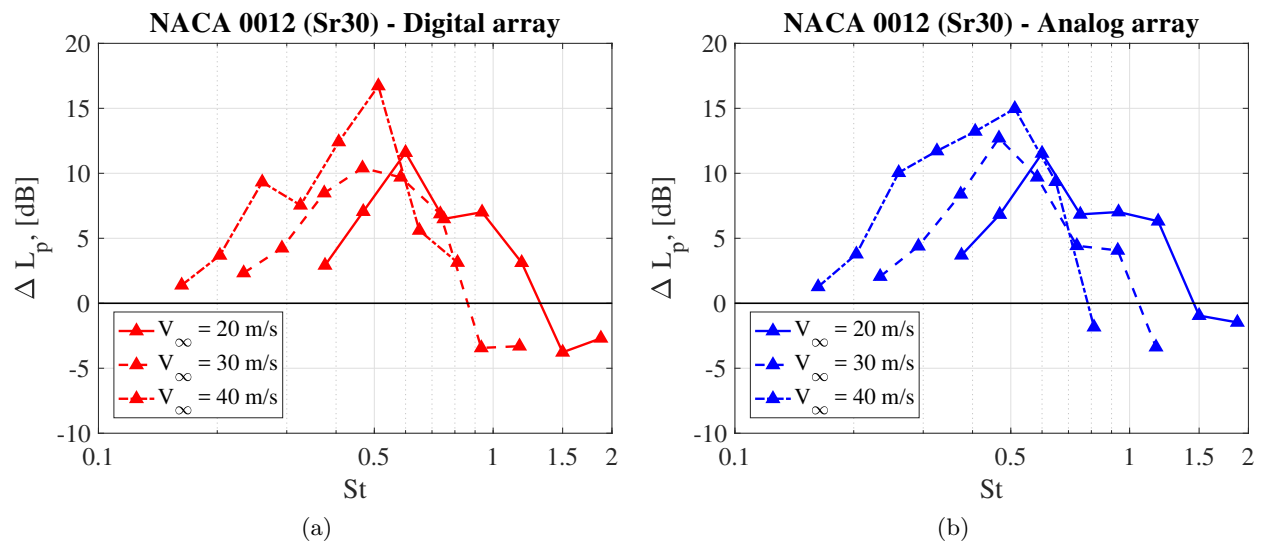


Figure 12: Relative integrated sound spectra with respect to the straight trailing edge for the NACA 0012 airfoil at  $\alpha = 0^\circ$  with respect to the Strouhal number  $St$  based on  $\delta_{95}$  for: (a) the *Digital* array. (b) the *Analog* array.

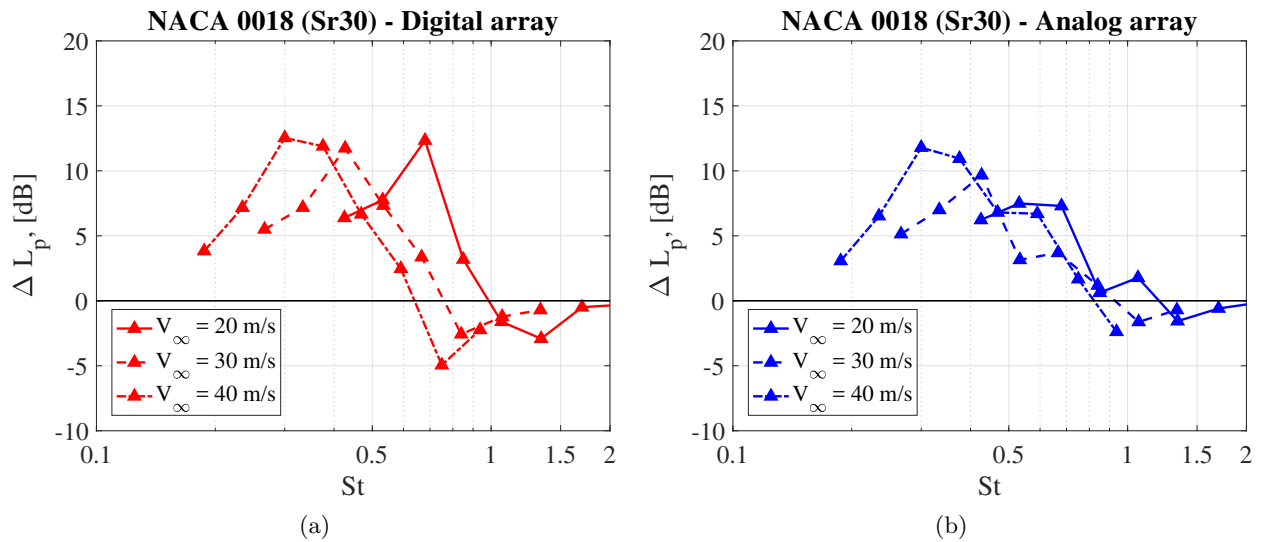


Figure 13: Relative integrated sound spectra with respect to the straight trailing edge for the NACA 0018 airfoil at  $\alpha = 0^\circ$  with respect to the Strouhal number  $St$  based on  $\delta_{95}$  for: (a) the *Digital* array. (b) the *Analog* array.

For both airfoils, the maximum noise reductions are obtained for a Strouhal number of about  $St \approx 0.5$  for both microphone arrays. This Strouhal number agrees well with the findings by Arce León et al. [25, 26]. In general, higher freestream velocities lead to higher noise reductions. For the NACA 0018 airfoil, the spectrum for the case of  $V_\infty = 20$  m/s measured by the *Digital* array (Fig. 13a) does not seem to collapse well with the spectra corresponding to the other two freestream velocities. Thus, there is a considerable spread in the values of the crossover Strouhal number. A better collapse is found for the *Analog* array results (Fig. 13b). The crossover Strouhal numbers in this case show a somewhat better agreement with the expected value of  $St \approx 1$  found by Gruber [47].

#### D. Comparison with literature results

The frequency spectra measured by both arrays for the NACA 0018 airfoil with straight trailing-edge at  $\alpha = 0^\circ$  and  $V_\infty = 40$  m/s were compared with the experimental results by Arce León et al. [25] and computational results by Avallone et al. [48] for the same airfoil and conditions, see Fig. 14. The results from literature were scaled to consider the same airfoil span  $b = 0.7$  m. The computational data were obtained by applying the Lattice Boltzmann Method [36, 49] and propagating the far-field solution using the Ffowcs Williams–Hawkings [50] analogy. Avallone et al. [48] and van der Velden [36] already showed the satisfactory agreement between these experimental and computational results.

It can be observed that the *Analog* array presents a closer agreement to the results from literature, especially to those from Arce León et al., with differences up to 3 dB. The *Digital* array, on the other hand, presents a similar trend but with slightly higher values (about 4 dB) with respect to the literature cases, especially at higher frequencies. The cause of this offset might be the higher presence of sidelobes for the *Digital* array results (see section A) which causes an increase in the numerator in Eq. (1), whereas the denominator remains constant.

Moreover, the predicted sound spectrum by the model for clean airfoils within turbulent flows developed by Lockard and Lilley and adapted by Dobrzynski [51, 52] for a straight wing of the same dimensions and at  $\alpha = 0^\circ$  and  $V_\infty = 40$  m/s, and same observer position, is also included in Fig. 14 for comparison. Similar orders of magnitude in the noise levels with respect to the experimental data are observed, but the predicted spectrum presents a lower decrease in levels for increasing frequencies. These differences can be explained because no information about the airfoil cross section is used by the method by Lockard and Lilley, which was originally developed considering flat plates [52].

The  $\Delta L_p$  values obtained with the *Analog* array (see section IV.C) show a better agreement with those obtained by Arce León et al. [25] and Avallone et al. [48], but, in general, higher noise reduction values are

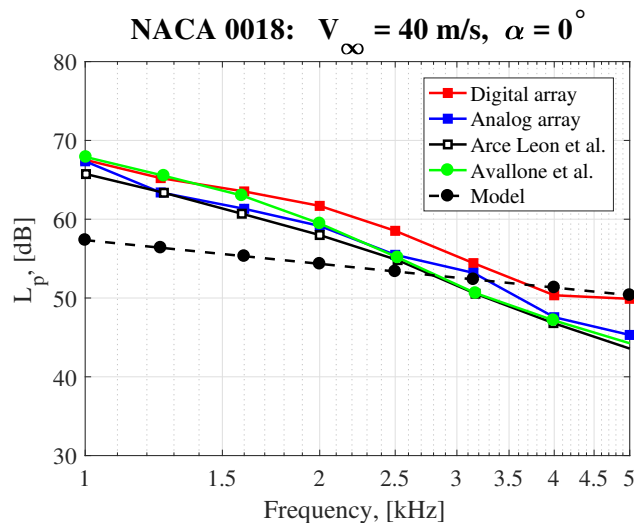


Figure 14: Integrated sound spectra for the NACA 0018 airfoil with straight trailing-edge at  $\alpha = 0^\circ$  and  $V_\infty = 40$  m/s measured by both arrays, experimental results by Arce León et al. [25], computational results by Avallone et al. [48] and predictions using the model by Lockard and Lilley [51] for the same airfoil and conditions.

measured in the current experiment. This is likely to be due to the considerably longer serration lengths used in this experiment, compared to the ones found in [25] and in [48], which were 10% and 20% of the airfoil chord (i.e., 2 and 4 cm), respectively. In general, longer serrations are expected to provide higher noise reductions [23].

### E. Correlation with flow velocity

As a last comparison between the results obtained by both microphone arrays, the correlation between the measured trailing-edge noise levels and the flow velocity  $V_\infty$  is investigated for both airfoils. Figure 15 presents the measured overall  $L_p$  values ( $L_{p,overall}$ ) values for the frequency range of interest and for the straight-trailing-edge baseline with respect to the flow velocity, as well as the expected 5<sup>th</sup> power law dependence of the acoustic power with the flow velocity for this type of sound sources [53, 54].

The  $L_{p,overall}$  results of both arrays are similar (with the *Digital* array results slightly about 2 dB higher) and agree very well with the 5<sup>th</sup> power law. The results of the NACA 0018 present a constant positive offset of approximately 2 dB with respect to those of the NACA 0012, which is explained by its higher thickness.

## V. Conclusions

The performances of two phased microphone arrays (one with digital MEMS microphones and the other with analog condenser microphones of similar cost) have been assessed in airfoil trailing-edge noise measurements. Two airfoils (NACA 0012 and NACA 0018) were tested in an open-jet wind tunnel and the performance of two different trailing-edge serration geometries was investigated.

Whereas the noise levels obtained by both arrays when using beamforming are very similar, the *Analog* array presented considerably less sidelobes (i.e., about 5 dB higher dynamic range) than the *Digital* array. The measured spectra agree well with similar studies from the literature. The noise reductions provided by the trailing-edge serrations (of more than 10 dB) and the dependence of the noise levels with the flow velocity are also in agreement with the theory.

Another difference between both arrays is that, according to the *Digital* array, the trailing-edge serrations seem to cause a noise increase after a threshold frequency of about 3.5 kHz, which is not expected from the theory or observed in similar experiments. The *Analog* array does not present such behavior. The differences in performance by the *Digital* array for frequencies higher than 3 kHz might be explained by the fact that

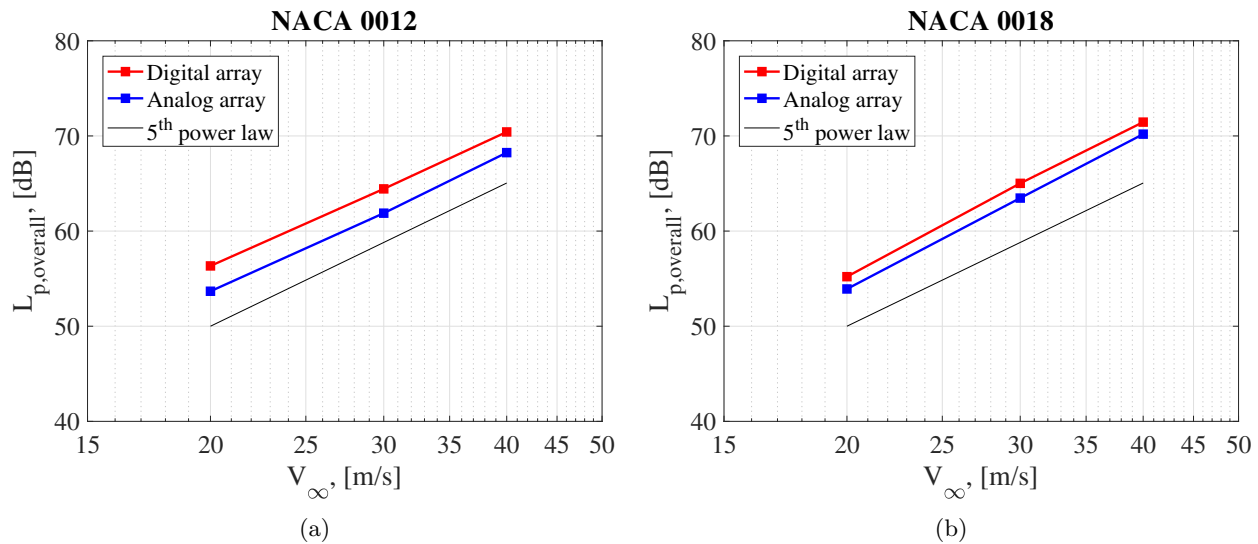


Figure 15:  $L_{p,overall}$  trailing-edge noise values measured by both arrays for the straight-trailing-edge case at  $\alpha = 0^\circ$  with respect to the flow velocity for: (a) NACA 0012 and (b) NACA 0018 airfoils.

digital MEMS microphones are usually optimized for the frequency range in human speech (300 Hz to 3 kHz).

In conclusion, the performance of both arrays seems to be similar for the cases analyzed here. The major advantages from the *Analog* array is the higher dynamic range in the beamform source plots and their better performance at higher frequencies ( $> 3$  kHz). The overall cost of a *Digital* array system is typically lower than an *Analog* one. Therefore, the hardware choice mostly depends on the frequency range of interest and the budget available.

## Acknowledgments

The authors would like to express their sincere gratitude to Steven Wanrooij and Herman Stobbe for their help and suggestions during the experimental campaign.

## References

- 1 Michel, U., Barsikow, B., Haverich, B., and Schüttelpelz, M., “Investigation of air-frame and jet noise in high-speed flight with a microphone array,” *3<sup>rd</sup> AIAA/CEAS Aeroacoustics Conference, May 12-14, 1997, Atlanta, GA, USA, 1997*, AIAA paper 1997-1596.
- 2 Merino-Martinez, R., Snellen, M., and Simons, D. G., “Functional beamforming applied to imaging of flyover noise on landing aircraft,” *Journal of Aircraft*, Vol. 53, No. 6, November–December 2016, pp. 1830–1843.
- 3 Merino-Martinez, R., Snellen, M., and Simons, D. G., “Functional Beamforming Applied to Full Scale Landing Aircraft,” *6<sup>th</sup> Berlin Beamforming Conference, February 29 – March 1 2016, Berlin, Germany, GfA, e.V., Berlin, 2016*, BeBeC-2016-D12.
- 4 Merino-Martinez, R., Bertsch, L., Snellen, M., and Simons, D. G., “Analysis of landing gear noise during approach,” *22<sup>nd</sup> AIAA/CEAS Aeroacoustics Conference. May 30 – June 1 2016. Lyon, France, 2016*, AIAA paper 2016-2769.
- 5 Merino-Martinez, R., Snellen, M., and Simons, D. G., “Determination of Aircraft Noise Variability Using an Acoustic Camera,” *23<sup>rd</sup> International Congress on Sound and Vibration, July 10 – 14 2016, Athens, Greece, 2016*.

- 6 Merino-Martinez, R., Neri, E., Snellen, M., Kennedy, J., Simons, D., and Bennett, G., “Comparing flyover noise measurements to full-scale nose landing gear wind-tunnel experiments for regional aircraft,” *23<sup>rd</sup> AIAA/CEAS Aeroacoustics Conference. June 5 – 9 2017. Denver, Colorado, USA*, 2017, AIAA paper 2017–3006.
- 7 Barsikow, B., King III, W. F., and Pfizenmaier, E., “Wheel/Rail Noise Generated by a High-Speed Train Investigated with a Line Array of Microphones,” *Journal of Sound and Vibration*, Vol. 118, 1987, pp. 99–122.
- 8 Barsikow, B., “Experiences with various configurations of microphone arrays used to locate sound sources on railway trains operated by the DB AG,” *Journal of Sound and Vibration*, Vol. 193, 1996, pp. 283–293.
- 9 Caldas, L. C., Greco, P. C., Pagani, C. C. J., and Baccalá, L. A., “Comparison of different techniques for rotating beamforming at the university of São Paulo fan rig test facility,” *6<sup>th</sup> Berlin Beamforming Conference, February 29 – March 1 2016, Berlin, Germany*, GFaI, e.V., Berlin, 2016, BeBeC–2016–D14.
- 10 Herold, G. and Sarradj, E., “Frequency domain deconvolution for rotating sources on an axial fan,” *6<sup>th</sup> Berlin Beamforming Conference, February 29 – March 1 2016, Berlin, Germany*, GFaI, e.V., Berlin, 2016, BeBeC–2016–D18.
- 11 Oerlemans, S. and Méndez López, B., “Acoustic Array Measurements on a Full Scale Wind Turbine,” *11<sup>th</sup> AIAA/CEAS Aeroacoustics Conference, May 23 – 25, 2005, Monterey, California, USA*, 2005, AIAA paper 2005–2963.
- 12 Oerlemans, S., *Detection of aeroacoustic sound sources on aircraft and wind turbines*, PhD thesis, University of Twente, Enschede, the Netherlands, 2009.
- 13 Merino-Martinez, R., Sijtsma, P., Snellen, M., Ahlefeldt, T., Antoni, J., Bahr, C., Blacodon, D., Ernst, D., Finez, A., Funke, S., Geyer, T., Haxter, S., Herold, G., Huang, X., Humphreys, W., Leclère, Q., Malgoezar, A., Michel, U., Padois, T., Pereira, A., Picard, C., Sarradj, E., Siller, H., Simons, D. G., and Spehr, C., “Aircraft Noise Generation and Assessment: A review of acoustic imaging methods using phased microphone arrays,” *CEAS Aeronautical Journal*, 2017, Accepted for publication.
- 14 Mueller, T., *Aeroacoustic Measurements*, Springer Science & Business Media, 2002, ISBN–978–3–642–07514–8.
- 15 Sijtsma, P., “Phased array beamforming applied to wind tunnel and fly-over tests,” Tech. Rep. NLR–TP–2010–549, National Aerospace Laboratory (NLR), Anthony Fokkerweg 2, 1059 CM Amsterdam, P.O. Box 90502, 1006 BM Amsterdam, The Netherlands, December 2010.
- 16 Alexandridis, A., Papadakis, S., Pavlidi, D., and Mouchtaris, A., “Development and evaluation of a digital MEMS microphone array for spatial audio,” *24<sup>th</sup> Signal Processing Conference (EUSIPCO). August 29 – September 2 2016. Budapest, Hungary*, 2016.
- 17 Herold, G. and Sarradj, E., “Microphone array method for the characterization of rotating sound sources in axial fans,” *Noise Control Engineering Journal*, Vol. 63, No. 6, 2015, pp. 546–551.
- 18 Yardibi, T., Zawodny, N. S., Bahr, C. J., Liu, F., Cattafesta III, L. N., and Li, J., “Comparison of microphone array processing techniques for aeroacoustic measurements,” *International Journal of Aeroacoustics*, Vol. 9, No. 6, 2010, pp. 733–762, SAGE Publications Ltd. London, United Kingdom.
- 19 Sarradj, E., Herold, G., Sijtsma, P., Merino-Martinez, R., Malgoezar, A. M. N., Snellen, M., Geyer, T. F., Bahr, C. J., Porteous, R., Moreau, D. J., and Doolan, C. J., “A microphone array method benchmarking exercise using synthesized input data,” *23<sup>rd</sup> AIAA/CEAS Aeroacoustics Conference. June 5 – 9 2017. Denver, CO, USA*, 2017, AIAA paper 2017–3719.
- 20 Herold, G., Geyer, T. F., and Sarradj, E., “Comparison of Inverse Deconvolution Algorithms for High-Resolution Aeroacoustic Source Characterization,” *23<sup>rd</sup> AIAA/CEAS Aeroacoustics Conference. June 5 – 9 2017. Denver, Colorado, USA*, 2017, AIAA paper 2017–4177.

- <sup>21</sup> Oerlemans, S., Fisher, M., Maeder, T., and Kögler, K., “Reduction of Wind Turbine Noise Using Optimized Airfoils and Trailing-Edge Serrations,” *AIAA Journal*, Vol. 47, No. 6, 2009, pp. 1470–1481.
- <sup>22</sup> Rubio Carpio, A., Merino-Martinez, R., Avallone, F., Ragni, D., Snellen, M., and van der Zwaag, S., “Broadband Trailing Edge Noise Reduction Using Permeable Metal Foams,” *46<sup>th</sup> International Congress and Exposition of Noise Control Engineering, 27–30 August, 2017, Hong Kong*, 2017.
- <sup>23</sup> Gruber, M., Joseph, P., and Chong, T., “On the mechanisms of serrated airfoil trailing edge noise reduction,” *17<sup>th</sup> AIAA/CEAS Aeroacoustics Conference (32<sup>nd</sup> AIAA Aeroacoustics Conference), 5 – 8 June 2011, Portland, Oregon, USA*, 2011, AIAA paper 2011–2781.
- <sup>24</sup> Finez, A., Jondeau, E., Roger, M., and Jacob, M., “Broadband Noise Reduction of a Linear Cascade With Trailing Edge Serrations,” *17<sup>th</sup> AIAA/CEAS Aeroacoustics Conference (32<sup>nd</sup> AIAA Aeroacoustics Conference), 5 – 8 June 2011, Portland, Oregon, USA*, 2011, AIAA paper 2011–2874.
- <sup>25</sup> Arce León, C., Merino-Martinez, R., Ragni, D., Avallone, F., and Snellen, M., “Boundary layer characterization and acoustic measurements of flow-aligned trailing edge serrations,” *Experiments in Fluids*, Vol. 57, No. 182, October 2016, pp. 1 – 22.
- <sup>26</sup> Arce León, C., Merino-Martinez, R., Ragni, D., Avallone, F., Scarano, F., Pröbsting, S., Snellen, M., Simons, D. G., and Madsen, J., “Effect of trailing edge serration-flow misalignment on airfoil noise emission,” *Journal of Sound and Vibration*, Vol. 405, May 2017, pp. 19 – 33.
- <sup>27</sup> Arce León, C., Merino-Martinez, R., Pröbsting, S., Ragni, D., and Avallone, F., “Acoustic Emissions of Semi-Permeable Trailing Edge Serrations,” *Acoustics Australia*, Vol. 1, 2017.
- <sup>28</sup> Arce León, C., Merino-Martinez, R., Ragni, D., Pröbsting, S., Avallone, F., Singh, A., and Madsen, J., “Trailing Edge Serrations – Effect of Their Flap Angle on Flow and Acoustics,” *7<sup>th</sup> International Meeting on Wind Turbine Noise, May 2 – 5 2017, Rotterdam, the Netherlands*, 2017.
- <sup>29</sup> Merino-Martinez, R., van der Velden, W. C. P., Avallone, F., and Ragni, D., “Acoustic measurements of a DU96-W-180 airfoil with flow-misaligned serrations at a high Reynolds number in a closed-section wind tunnel,” *7<sup>th</sup> International Meeting on Wind Turbine Noise, May 2 – 5 2017, Rotterdam, the Netherlands*, 2017.
- <sup>30</sup> Avallone, F., van der Velden, W. C. P., Merino-Martinez, R., and Ragni, D., “Near-wall pressure fluctuations over noise reduction add-ons,” *23<sup>rd</sup> AIAA/CEAS Aeroacoustics Conference. June 5 – 9 2017. Denver, CO, USA*, 2017, AIAA paper 2017–4171.
- <sup>31</sup> Ragni, D., Avallone, F., and van der Velden, W. C. P., “Concave serrations on broadband trailing-edge noise reduction,” *23<sup>rd</sup> AIAA/CEAS Aeroacoustics Conference. June 5 – 9 2017. Denver, Colorado, USA*, 2017, AIAA paper 2017–4174.
- <sup>32</sup> Oerlemans, S., “Reduction of Wind Turbine Noise using Blade Trailing Edge Devices,” *22<sup>nd</sup> AIAA/CEAS Aeroacoustics Conference. May 30 – June 1 2016. Lyon, France*, 2016, AIAA paper 2016–3018.
- <sup>33</sup> Braslow, A. L., Hicks, R. M., and Harris Jr., R. V., “Use of grit-type boundary-layer transition trips on wind-tunnel models,” Tech. Rep. NASA-TN-D-3579, NASA Technical Note (D-3579), September 1966.
- <sup>34</sup> CAE Systems website, “<https://www.cae-systems.de/en/products/acoustic-camera-sound-source-localization/bionic-m-112.html>,” Accessed in January 2017.
- <sup>35</sup> PUI Audio POM-2735P-R microphone website, “<http://www.puiaudio.com/product-detail.aspx?categoryId=4&partnumber=POM-2735P-R>,” Accessed in January 2017.
- <sup>36</sup> van der Velden, W. C. P., *Computational aeroacoustic approaches for wind turbine blade noise prediction*, Ph.D. thesis, Delft University of Technology, 2017, ISBN 978–94–6186–756–8.
- <sup>37</sup> Welch, P. D., “The Use of Fast Fourier Transform for the Estimation of Power Spectra: A Method Based on Time Averaging Over Short, Modified Periodograms,” *IEEE Transactions on Audio and Electroacoustics*, Vol. AU–15, No. 2, June 1967, pp. 70–73.

- <sup>38</sup> Merino-Martinez, R., Sijtsma, P., and Snellen, M., “Inverse Integration Method for Distributed Sound Sources,” *7<sup>th</sup> Berlin Beamforming Conference, March 5 – 6 2018, Berlin, Germany*, GfAI, e.V., Berlin, 2018, BeBeC–2018–S07.
- <sup>39</sup> Brooks, T. F. and Humphreys, W. M., “Effect of Directional Array Size on the Measurement of Airframe Noise Components,” *5<sup>th</sup> AIAA/CEAS Aeroacoustics Conference. Bellevue, WA, USA*, 1999, AIAA paper 1999–1958.
- <sup>40</sup> Amiet, R. K., “Refraction of sound by a shear layer,” *Journal of Sound and Vibration*, Vol. 58, No. 4, 1978, pp. 467–482.
- <sup>41</sup> Tuinstra, M. and Sijtsma, P., “Suppression of spurious noise sources in airfoil self-noise measurements,” *21<sup>st</sup> AIAA/CEAS Aeroacoustics Conference. June 22 – 26 2015. Dallas, TX, USA*, 2015, AIAA paper 2015–2689.
- <sup>42</sup> Pagani, C. C. J., Souza, D. S., and Medeiros, M. A. F., “Slat Noise: Aeroacoustic Beamforming in Closed-Section Wind Tunnel with Numerical Comparison,” *AIAA Journal*, Vol. 54, No. 7, April 2016, pp. 2100–2115.
- <sup>43</sup> Lord Rayleigh, F. R. S., “XXXI. Investigations in Optics with special reference to the Spectroscope,” *The London, Edinburgh and Dublin Philosophical Magazine and Journal of Science*, Vol. 8, No. 49, October 1879, pp. 261–274.
- <sup>44</sup> Sijtsma, P., Merino-Martinez, R., Malgoezar, A. M. N., and Snellen, M., “High-Resolution CLEAN-SC: Theory and Experimental Validation,” *International Journal of Aeroacoustics*, Vol. 16, No. 4–5, 2017, pp. 274–298, SAGE Publications Ltd. London, United Kingdom.
- <sup>45</sup> Sarradj, E., “A generic approach to synthesize optimal array microphone arrangements,” *6<sup>th</sup> Berlin Beamforming Conference, February 29 – March 1 2016, Berlin, Germany*, GfAI, e.V., Berlin, 2016, BeBeC–2016–S4.
- <sup>46</sup> Howe, M. S., “Aerodynamic noise of a serrated trailing edge,” *Journal of Fluids and Structures*, Vol. 5, No. 1, January 1991, pp. 33–45.
- <sup>47</sup> Gruber, M., *Airfoil noise reduction by edge treatments*, Ph.D. thesis, University of Southampton, 2012.
- <sup>48</sup> Avallone, F., van der Velden, W. C. P., Ragni, D., and Casalino, D., “Noise reduction mechanisms of sawtooth and combed-sawtooth trailing-edge serrations,” *Journal of Fluid Mechanics*, 2018, Accepted for publication (doi: 10.1017/jfm.2018.377).
- <sup>49</sup> Succi, S., *The Lattice Boltzmann Equation For Fluid Dynamics and Beyond*, Clarendon Press, 1st ed., 2001, ISBN 9780198503989.
- <sup>50</sup> Ffowcs Williams, J. E. and Hawkings, D. L., “Sound generation by turbulence and surfaces in arbitrary motion,” *Philosophical Transactions of the Royal Society of London A – Mathematical, Physical and Engineering Sciences*, Vol. 264, No. 1151, May 1969.
- <sup>51</sup> Lockard, D. P. and Lilley, G. M., “The Airframe Noise Reduction Challenge,” Tech. Rep. NASA TM–2004–213013, NASA TM–2004–213013, 2004.
- <sup>52</sup> Bertsch, L., *Noise Prediction within Conceptual Aircraft Design*, Ph.D. thesis, DLR, 2013, DLR Forschungsbericht, ISRN DLR–FB–2013–20, ISSN 1434–8454.
- <sup>53</sup> Ffowcs Williams, J. E. and Hall, L. H., “Aerodynamic sound generation by turbulent flow in the vicinity of a scattering half plane,” *Journal of Fluid Mechanics*, Vol. 40, No. 4, 1970, pp. 657–670.
- <sup>54</sup> Fink, M. R., “Noise component method for airframe noise,” *4<sup>th</sup> AIAA Aeroacoustics Conference. October 3 – 5 1977, Atlanta, Georgia, USA*, 1977, AIAA Paper 1977–1271.